On Untethered, Dual Magneto- and Photoresponsive Liquid Crystal Bilayer Actuators Showing Bending and Rotating Motion

Pilz da Cunha, Marina; Foelen, Yari; Engels, Tom A.P.; Papamichou, Kleopatra; Hagenbeek, Michiel; Debije, Michael G.; Schenning, Albert P.H.J.

DOI
10.1002/adom.201801604

Publication date
2019

Document Version
Final published version

Published in
Advanced Optical Materials

Citation (APA)
Pilz da Cunha, M., Foelen, Y., Engels, T. A. P., Papamichou, K., Hagenbeek, M., Debije, M. G., & Schenning, A. P. H. J. (2019). On Untethered, Dual Magneto- and Photoresponsive Liquid Crystal Bilayer Actuators Showing Bending and Rotating Motion. *Advanced Optical Materials*, *7*(7), Article 1801604. https://doi.org/10.1002/adom.201801604

ADVANCED OPTICAL MATERIALS

www.advopticalmat.de

On Untethered, Dual Magneto- and Photoresponsive Liquid Crystal Bilayer Actuators Showing Bending and Rotating Motion

Marina Pilz da Cunha, Yari Foelen, Tom A. P. Engels, Kleopatra Papamichou, Michiel Hagenbeek, Michael G. Debije, and Albert P. H. J. Schenning**

The integration of untethered, multi-stimuli responsive actuation into soft microrobotic devices is a goal in the development of "smart" materials. This manuscript reports on a dual-stimuli responsive bilayer actuator consisting of a light responsive liquid crystal network (LCN) and a magnetic responsive polydimethylsiloxane (PDMS) composite. This design is of facile fabrication with ample design freedom, using no additional adhesion layers. Untethered control of the bilayer permits motions including bending and rotation, steered individually or in synchronization. Through a systematic study the direct impact of the PDMS layer was elucidated on the light triggered rate of actuation and maximum deformation amplitude of the LCN film. The alignment (homeotropic or planar) of the LCN has a profound effect on the resulting bilayer actuation. It is demonstrated, both experimentally and theoretically, that the rates of sample heating and actuation are directly correlated and highlight the critical role of the PDMS as a heat sink. The maximum amplitude of displacement of the bilayer is tied to the stiffness, being inversely correlated to the PDMS thickness to the third power. These results give insights and provide straightforward design rules to fabricate bilayer actuators with programmed multi-responsive properties.

1. Introduction

Nature exhibits many stimuli-responsive systems and organisms with a high degree of complexity, efficiency, and functionality.[1] In contrast, man-made materials are mostly static and do not adapt to changes in the environment. The next generation of synthetic materials will take inspiration from nature and incorporate stimuli-responsive behavior, expanding the archetypes of material functionality. Remote driving of materials through light,[2–5] pH,[6] and magnetic fields[7] are topics of current research, as untethered control will free devices from external wiring, increasing their versatility. Potential application of such materials includes soft robotics,[8–10] medical applications,[11,12] sensors,[13] and smart textiles.[14,15]

A common approach to stimuli-responsive, "smart" materials are employing bilayers in which deformations such as bending are caused by the differing

M. Pilz da Cunha, Y. Foelen, Dr. M. G. Debije,
Prof. A. P. H. J. Schenning
Laboratory of Stimuli-responsive Functional Materials & Devices
Department of Chemical Engineering and Chemistry
Eindhoven University of Technology
P.O. Box 513, 5600 MB Eindhoven, The Netherlands
E-mail: m.g.debije@tue.nl; a.p.h.j.schenning@tue.nl

M. Pilz da Cunha, Prof. A. P. H. J. Schenning
Institute for Complex Molecular Systems
Eindhoven University of Technology
Den Dolech 2, 5600 MB Eindhoven, The Netherlands

The ORCID identification number(s) for the author(s) of this article can be found under https://doi.org/10.1002/adom.201801604.

DOI: 10.1002/adom.201801604

Dr. T. A. P. Engels
Department of Mechanical Engineering
Materials Technology Institute
Eindhoven University of Technology
P. O. Box 513, 5600 MB Eindhoven, The Netherlands

K. Papamichou
Laboratory of Novel Aerospace Materials
Delft University of Technology
Kluyverweg 1, 2629 HS Delft, The Netherlands

Dr. M. Hagenbeek
Laboratory of Structural Integrity & Composites
Delft University of Technology
Kluyverweg 1, 2629 HS Delft, The Netherlands

Prof. A. P. H. J. Schenning
SCNU-TUE Joint Laboratory of Device Integrated Responsive Materials (DIRM)
South China Normal University
Guangzhou Higher Education Mega Center
510006 Guangzhou, China

properties of the two constituent materials.[16] By combining a passive and a responsive material, macroscopic deformations can be triggered via exposure to a stimulus that causes expansion/shrinkage of the active material layer. The passive material acts as a resistance to the volumetric changes, leading to reversible actuation upon removal of the stimulus.[17] Responsive materials in such bilayer designs include hydrogels and liquid crystalline polymers.[18]

Liquid crystalline networks (LCNs) that show responsive behavior to light,[19–23] temperature,[24–26] humidity,[27,28] or magnetic fields[29,30] have attracted considerable attention for their potential as smart functional materials, as their response can be programmed and they may be operated in dry environments. Present works demonstrate possible combination of responsive LCN films with passive polymer materials such as polyethylene (PE),[31,32] polypropylene (PP),[33] polyamide-6 (PA6),[34,35] and polystyrene (PS).[36] These bi/multilayered smart materials will present altered stimuli-responsive behavior when compared to single layer LCN actuators due to different mechanical and thermal properties. Studies of thermally triggered deformations of bimetal materials have been documented in detail,[37] yet no detailed study is available that illustrates the effect the additional layer has on the actuation rate of stimuli-responsive liquid crystal-based bilayers. Detailed analysis and understanding of the effects that additional layers have on the triggered deformation of the responsive systems is vital for the design of bi/multilayer actuator devices with programmed responsive properties.

Bilayer designs offer the possibility for the integration of different stimuli responsive behaviors into single devices. By functionalizing the otherwise passive layer, multi-responsive materials can be developed. Integration of multi-triggered response into a single device is of specific interest for soft microrobotic applications. Additionally, untethered multi-stimuli response in soft robotics can allow for controlled actuation that involves independent stimuli triggering different motions, such as bending and rotating, expanding the versatility of the device.

In our previous work, we revealed the mechanism for the light triggered response of a liquid crystal network doped with a fast isomerizing azobenzene.[38] The single films studied display an unbending actuation upon illumination from a precurled shape into an extended film, the actuation motion independent from the illumination direction. We have shown that the photoresponsive deformation is caused by an interplay of photothermal and photosoftening effects, in which anisotropic thermal expansion is the governing factor. A clear match between heating and deformation timescales shows the dominant effect of temperature on establishing the actuation rate for photothermal LCN systems.

Here, we present a novel, easily fabricated multi-stimuli responsive bilayer consisting of a photothermal LCN and magnetic polydimethylsiloxane (PDMS), requiring no additional adhesion layers and with ample design freedom (**Figure 1**A). The magnetic- and light-triggered responses of the bilayer can individually lead to different mechanical motions, with light triggering unbending, and a magnetic field allowing for rotational freedom through magnetic guidance (Figure 1B).[11] With two different, independent stimuli-triggered motions, the bilayer can perform two actuation mechanisms in synchronization. Furthermore, we demonstrate that exposing the bilayer to a sufficiently strong magnetic field allows for induction heating to activate bending of the bilayer directly (**Figure 2**).

We elucidate the effects of PDMS layers of varying thicknesses on the photoresponsive actuation of the liquid crystal films

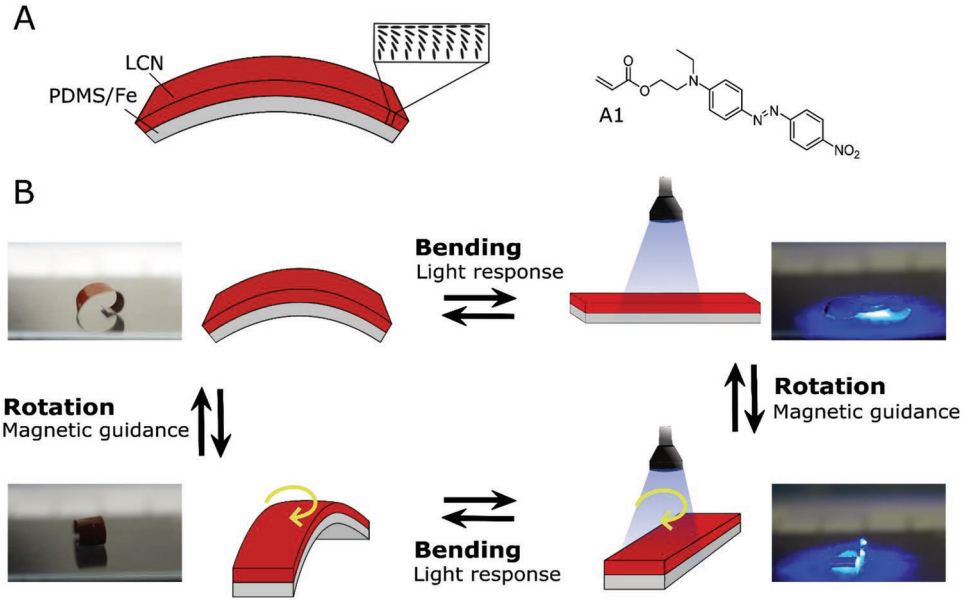

Figure 1. A) Schematic of the bilayer design, composed of a splay aligned azobenzene doped LCN and a magnetic PDMS coated onto the homeotropic surface of the LCN: A1 is the photoresponsive azobenzene derivative within the liquid crystal network. B) Schematic representation and images of the bilayer during actuation as a response to two different stimuli: light and a magnetic field. Without illumination, the bilayer has a bent shape. Upon illumination (455 nm) the material unbends and becomes flat. A simple refrigerator magnet is employed to address the film either subsequent to or during the light exposure. The magnetic response allows for rotation or positional freedom of the bilayer.

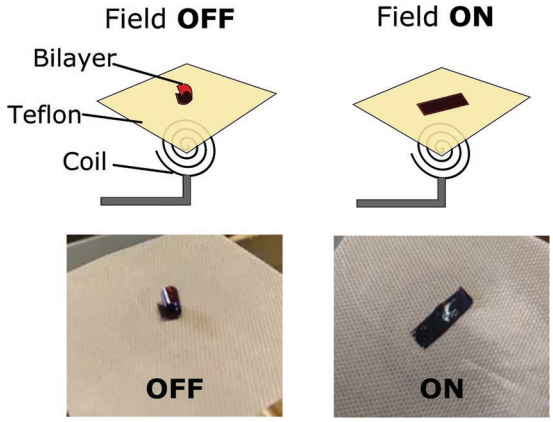

Figure 2. Bilayer film of an LCN and PDMS containing iron fillers in 1:1 weight ratio (35 μm) shows response to strong magnetic field. Unbending motion is observed upon application of the stimulus; the mechanism of unbending is due to induction heating of the bilayer caused by the magnetic particles in the PDMS.

through a detailed video and thermal analysis. We demonstrate that incorporating magnetic particles into the PDMS layer imposes minimal impedance of the photoactuation. We shed light on the effects governing the device's maximum deformation amplitudes and rates through an experimental as well as a theoretical approach, providing a design toolbox for future multi-responsive, multi-functional bilayer actuators.

2. Results and Discussions

2.1. Preparation of the Bilayer Actuator

The bilayer actuator consists of a photoresponsive LCN (20 μm in thickness) and a PDMS layer of varying thicknesses (50, 130, and 210 μm). The liquid crystal polymer is a splay aligned network, composed of two LC monomers (M1, 56.5 mol% and M2, 40.5 mol%,), a photo responsive azobenzene dopant (A1, 2 mol%) and a photoinitiator (PI, 1 mol%) (Figure S1, Supporting Information): film preparation follows previously reported methods.[38] In splay alignment, the LC molecules at the opposing surfaces of the film have different orientations: one has a planar alignment in which the molecules are oriented parallel to the surface, and the other a homeotropic with molecules aligned perpendicular to the surface (Figure 1A). This hybrid alignment allows for uniform and well-controlled photothermal bending deformations, with a higher magnitude of actuation via opposing expansion coefficients on opposite surfaces of the film, maximizing deformation when compared to other alignment configurations, such as antiparallel and homeotropic alignments.[39,40] Due to the elevated polymerization temperature of the network, anisotropic molar volume shrinkage results in a film that has a bent shape at room temperature, with the homeotropic side of the splay on the inside of the curl.

The magnetic PDMS composite is fabricated through manual mixing of carbonyl iron particles with uncured PDMS at a 1:1 weight ratio. Subsequent degassing of PDMS or PDMS composite releases air bubbles trapped during mixing. The bilayer is constructed by applying the PDMS or PDMS composite onto the LCN by either blade coating (thicknesses 50, 130, and 210 μm), or spin coating (35 μm) of the uncured PDMS layer directly onto the LCN. Subsequent curing of the PDMS is performed at 80 °C for 1 h and the resulting bilayer shows no delamination issues.

2.2. Stimuli Responsive Behavior

Our dual stimuli responsive actuator consists of a light responsive liquid crystal network (20 μm) and a magnetic responsive PDMS (35 μm) made through incorporation of iron particles into the PDMS layer (vide supra, Figure 1A). Creation of the composite material (PDMS/Iron) with a 1:1 weight ratio is possible without significant increase of the composite's modulus (Figure S2, Supporting Information). The dual response of the device allows for two modes of motion: light triggered or magnetic field induced bending, and rotational freedom through magnetic response (Figure 1B and Figure 2).

2.2.1. Magnetic Field Induced Unbending Actuation

Exposure of the bilayer to sufficiently strong magnetic fields resulted in unbending actuation (Figure 2). The actuation is a result of temperature increase in the device due to induction heating of the magnetic PDMS. Upon heating, the liquid crystal network in the bilayer shows anisotropic thermal expansion due to its splay molecular alignment. The anisotropic expansion results in the macroscopic unbending of the device. Upon application of the magnetic field (800 Oe, 0.08 T) the bilayer reached close to 55 °C within a few seconds and the corresponding unbending actuation was observed (details found in the Experimental Section).

2.2.2. Dual Magnetic and Light Responsive Behavior

With two independent stimuli-triggered motions, the bilayer can perform two actuation mechanisms in synchronization. Unbending and rotational motion of the bilayer, as shown in Figure 1B, can be addressed by light and magnetic guidance respectively. Prior to illumination, the bilayer has a bent shape with the magnetic PDMS found on the inside of the curvature, whereas upon illumination the liquid crystal layer actuates, leading to bilayer unbending. Magnetic triggered rotational motion of the bilayer can be addressed subsequent to or in synchronization with the illumination, Movie S1 in the Supporting Information. Whereas the magnetic response of the bilayer is simply employed through magnetic guidance with another magnet, the light responsive behavior is more complex, with strong variations depending on the design construction and bilayer thickness.

2.3. Photoresponsive Actuation Analysis of LCN/PDMS Bilayers

To study the photo actuation of the bilayer, we first compared the actuation of films coated with PDMS on the planar and

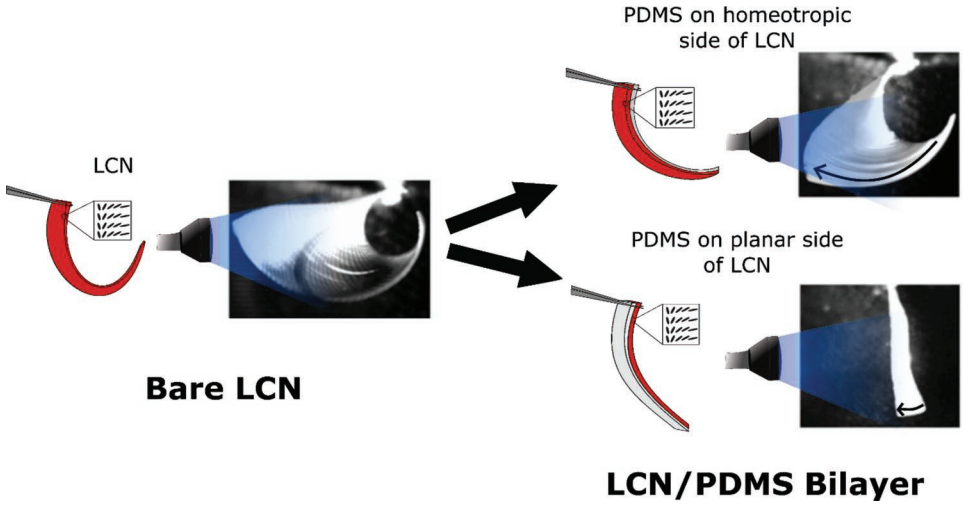

Figure 3. Upon illumination, a bare LCN actuates by unbending from a prebent shape into an extended film. The samples are illuminated from the left with the planar side of the splay facing the light: the film bends towards the light source. Once PDMS (130 µm) is coated onto one of the LCN surfaces (homeotropic or planar), actuation is altered with coating on the planar side showing the largest resistance to actuation. Images are generated by overlaying individual frames of a video taken during the illumination.

on the homeotropic surfaces of the splay aligned LCN. Upon exposure to light, the LCN (which has a bent shape at room temperature), actuates by extending from the prebent shape into a stretched film. Analysis of this actuation is performed by filming the bilayer during light exposure and following the end-point of the films to generate time dependent displacement image stacks of the maximum bilayer actuation. These stacked images demonstrate the magnitude of deformation and show the path followed by the bilayer during actuation. As PDMS is transparent to the 455 nm light used for actuation, and the photoresponse is independent from illumination direction, all samples were positioned so that the planar side of the LCN is facing the light. As demonstrated by **Figure 3**, the LCN surface (planar or homeotropic) onto which PDMS is coated has a dramatic effect on the actuation of the bilayer. When coated onto the planar surface of the LCN, PDMS dramatically inhibits deformation, causing significant reduction in the prebending of the bilayer prior to illumination. However, when placed on the homeotropic surface, the film responds to light by unbending from its precurled shape to an extended film, very similar to the actuation seen for a bare LCN. The importance of the surface onto which PDMS should be coated is due to the effective volumetric changes occurring at the two different sides of the LCN; contraction at planar surface and expansion on the homeotropic side. At elevated temperatures, the planar side of the LCN contracts whereas PDMS expands, resulting in opposing forces at the layer interface. This is also the reason for the reduced prebend: cooling down from polymerization temperature to room temperature results in expansion of the planar side of the splay LC film while the PDMS contracts.

We studied the effect of PDMS layer thickness on the photoactuation through analysis of 50, 130, and 210 µm thick PDMS bilayer films coating the homeotropic side of the LCN. The image stacks (top of **Figure 4**) show that the addition of

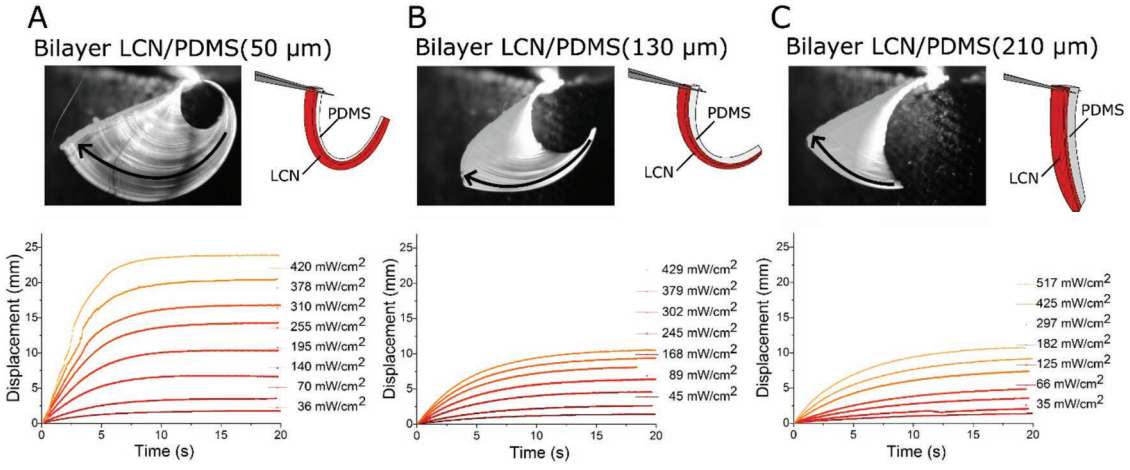

Figure 4. End-point displacement evolution plot for bilayers of LC/PDMS with PDMS thickness of A) 50 µm, B) 130 µm, and C) 210 µm in response to 455 nm light of varied incident energy intensities. Top figures show stacked images of the actuation of the bilayers at highest energy intensity (with illumination coming from the left).

PDMS layers result in a different initial prebend of the bilayer in its nonilluminated state. The change in prebend is a result of the greater stiffness of the thicker PDMS layer, which resists the initial curling of the LCN normally seen at room temperature when the system is cooled after being polymerized at high temperature. This effect plays a role in the design of such bilayer devices, as the range of physical motions can be affected by the presence of the PDMS layer, in terms of both thickness of the attached layer and the area covered by the PDMS.

The actuation rate of the bilayers is depicted as displacement plots, in which the movement of the tip of the bilayer is tracked over time; see Figure 4. Congruent to the deformation analysis, the temperature evolution of the bilayers during actuation was recorded. This systematic study combines deformation and thermal analysis, shedding light on the impact of bilayer thickness on the device's rate of deformation and maximum displacement amplitude. Comparing the actuation rate of the bilayers, Figure 4, and the bare LCN film, Figure S3 (Supporting Information), a clear change in actuation rate is observed. The presence of a PDMS layer slows the actuation of the device; increase of the PDMS thickness from 50 to 210 µm further reduces the deformation rate. Furthermore, the impact of PDMS on the actuation of the bilayer is also clearly seen in terms of maximum deformation amplitude, decreasing substantially upon increase of PDMS layer thickness from 50 to 130 µm, Figure 4A,B.

2.4. Bilayer Effect on the Rate of Deformation

Just as previously established for the single LCN system, the rate at which the bilayers deform upon illumination is also directly connected to the rate at which the device heats up, **Figure 5**A. When comparing the heating rate of the bilayer to the single LCN in Figure 5A, it can be observed that even though the two systems reach similar temperatures after extended illumination time, the rate at which the two systems heat up is very different. The heating of the bilayer is slowed as the PDMS acts as a heat sink, increasing the volume over which the heat generated by the azo-benzene molecule in the LCN is distributed. In Figure 5B and Table S1 (Supporting Information) we show that a change in the PDMS thickness, from 50 to 130 µm or 130 to 210 µm, results in a large decrease in the rate of deformation of the system; the heating rate decrease is consistent over several illumination energy intensities.

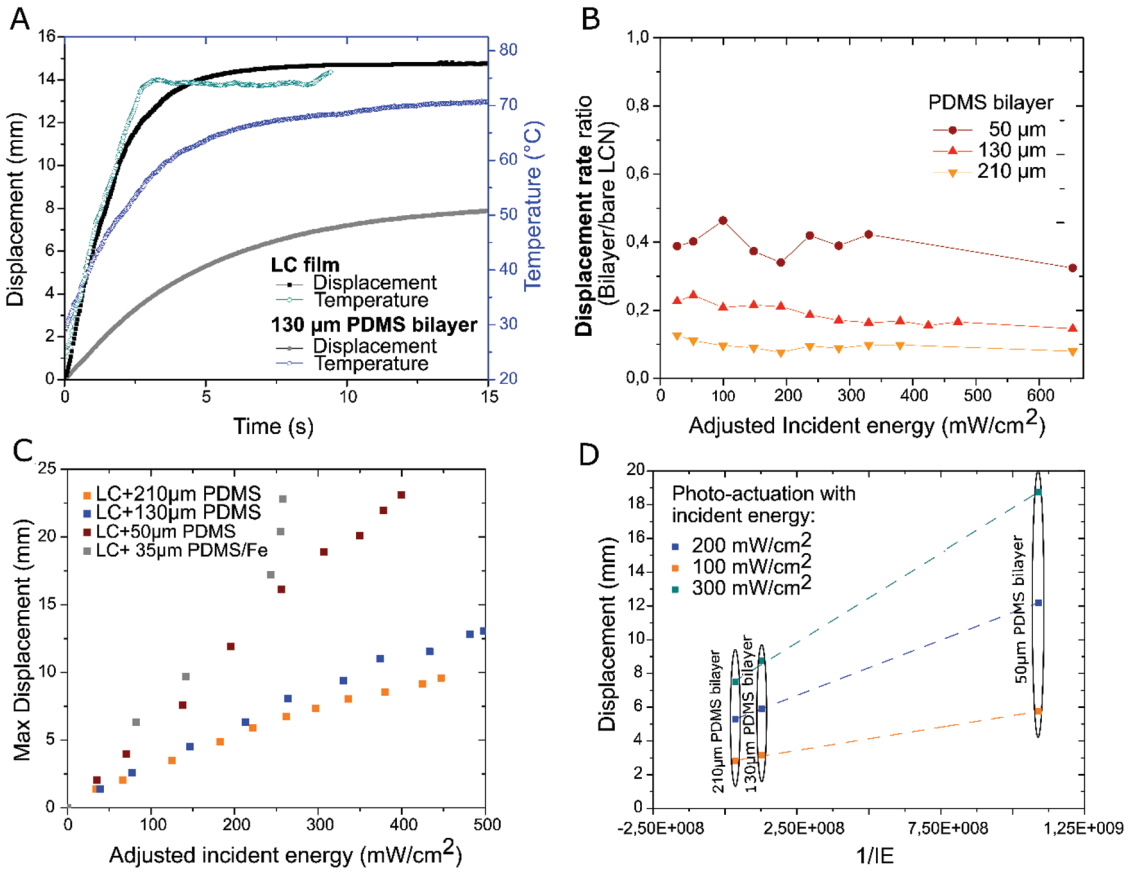

Figure 5. A) Variations in the timescale of deformation for the 130 µm bilayer when compared to the LC film (illumination at 260 mW cm^{-2}), displaying the clear connection between sample heating and displacement. B) Displacement rate ratio of the different bilayers during the initial seconds of deformation, at varied incident light energies when compared to the bare LCN prior to bilayer coating. C) Maximum end-point displacement for four bilayers with differing PDMS thicknesses, as a function of the incident energy intensity. D) Scaling between displacement and inverse of bending modulus ($1/IE$) at three different illumination energies for the three different bilayers. The linearity between displacement and the value of $1/IE$ further supports our scaling guidelines, highlighting the impact material stiffness has on the final deformation.

A simplified heat balance for the system can be written as

$$P_{heat} = P_{absorb} - P_{cool} \quad (1)$$

in which P_{absorb} is the total heat absorbed by the LCN and P_{cool} the convective heat loss to the surroundings. $P_{cool} = 2hA(T_{max} - T_0)$ and $P_{heat} = c_p \cdot m \cdot \dot{T}$, with A being the surface area of the film (assuming the heat loss along the thin edges of the film to be negligible), T_{max} and T_0 the maximum and initial film temperatures, respectively, h the convective heat transfer coefficient, and c_p the specific heat and m the mass of the system. Rewriting Equation (1)

$$c_p \cdot m \cdot \dot{T} = P_{absorb} - h \cdot 2A \cdot (T_{max} - T_0) \quad (2)$$

Equation (2) can be recast as a standard first order inhomogeneous differential equation

$$\dot{T} = BT + C \quad (3)$$

where $B = \frac{-h}{c_p \cdot d \cdot \rho}$, and $C = \frac{P_{absorb} + h \cdot 2A \cdot T_0}{c_p \cdot A \cdot d \cdot \rho}$, $m = d \cdot A \cdot \rho$, where ρ is the material density and d the film thickness.

The solution of the differential equation with the boundary condition at $t = 0$; $T(t) = T_0$ is

$$T(t) = T_0 + \frac{P_{absorb}}{h \cdot 2A}\left(1 - e^{\frac{-2h}{c_p \cdot d \cdot \rho} \cdot t}\right) \quad (4)$$

Thus, as the thickness, d, of the system increases, the exponential term decreases and the heating time, $T(t)$, increases. This expression supports our experimental observation of increasing heating times when adding PDMS to a bare LCN.

When the temperature of the system reaches equilibrium

$$P_{absorb} = P_{cool} \quad (5)$$

The equilibrium balance in Equation (5) can be rewritten, taking $P_{cool} = 2hA\ (T_{max} - T_0)$.

$$T_{max} = T_0 + \frac{P_{absorb}}{h \cdot 2A} \quad (6)$$

For simplicity, in the heat balance constructions we assume specific heat capacity of the LCN and PDMS to be equal: small deviations in the specific heat capacities would result in small systematic differences in the final temperature at equilibrium. Therefore, for long illumination times, both bilayers and bare LCNs should reach similar equilibrium temperatures when exposed to the same illumination intensity, as the maximum temperature at equilibrium is independent of thickness, just as observed experimentally (Figure 5A).

2.5. Bilayer Effect on the Maximum Deformation Amplitude

The decreased maximum deformation amplitude for thicker bilayers, Figure 5C, is caused by an increased stiffness of the system.[37] We observe that a thin (50 µm) PDMS layer coated onto the photoresponsive 20 µm LCN shows minimal hinderance of the maximum amplitude attained: Figure S3 (Supporting Information) versus Figure 4. However, further increasing the PDMS thickness (to 130 or 210 µm) results in similar deformation amplitudes but require increasingly higher light energy inputs.

Considering the LCN as a cantilever, the actuation force is directly dependent on the bending modulus, EI, with I the moment of inertia and E Young's modulus. The displacement of the end point of a beam scales inversely with the bending modulus.

$$\Delta x \sim \frac{1}{\widetilde{EI}} \quad (7)$$

with $\widetilde{EI}$ being the effective bending modulus, which for the bilayer we consider both a PDMS and an LCN layer, including individual thicknesses (d_{PDMS}, d_{LC}) and moduli (E_{PDMS}, E_{LC})

$$\widetilde{EI} = \frac{w d_{PDMS}^3 d_{LC} E_{PDMS} E_{LC}}{12(d_{LC}E_{LC} + d_{PDMS}E_{PDMS})} K \quad (8)$$

where

$$K = 4 + 6\frac{d_{LC}}{d_{PDMS}} + 4\left(\frac{d_{LC}}{d_{PDMS}}\right)^2 + \frac{E_{LC}}{E_{PDMS}}\left(\frac{d_{LC}}{d_{PDMS}}\right)^3 + \frac{E_{PDMS}}{E_{LC}}\frac{d_{PDMS}}{d_{LC}} \quad (9)$$

The layer thickness has an important impact on the effective bending modulus, and the displacement of the end of the bilayer cantilever is expected to be approximately proportional to the layer thickness by d^3.

As a toolbox for future bilayer designs, we suggest that estimations on photoactuated displacement of bilayers can be made with prior knowledge of the bilayer's bending modulus. A display of the linear scalability between bending modulus and bilayer displacement is shown in Figure 4D for three different bilayers at similar incident energies. Thin layers of PDMS are observed to cause almost no inhibition of actuation, while thicker layers dramatically reduce the maximum deformation due to increased material stiffness. A careful selection of PDMS thickness is required to adequately balance strength and desired bending characteristics in LCN/PDMS bilayer actuators.

We observed that the additional weight from the iron fillers in a thin bilayer (35 µm PDMS) does not result in a decrease of maximum amplitude of actuation. When exposed to light, the dual responsive bilayer shows little impediment in the photoactuation amplitude when compared to a thin PDMS/LCN bilayer (50 µm), Figure 5C, or to the bare LCN, Figure S3 in the Supporting Information. Similarly, the temperature evolution of the composite bilayer is unaltered when compared to the same thickness bilayer without magnetic fillers, Figure S4 in the Supporting Information. These findings show that additional layers with low stiffness do not pose limitations to the functioning of a photoresponsive liquid crystal actuator, and yet can be designed to add a stimuli response to the device.

3. Conclusions

We present a systematic study of a bilayer composed of a splay aligned photoresponsive LC film coupled with a flexible PDMS layer of three different thicknesses. We illustrate the impact of the PDMS layer on the light responsive actuation of the bilayer, considering both rates of displacement and maximum amplitude

of deformation. In connection to previous studies, we establish a direct correlation between heating rates and displacement rates, which are decreased in the presence of a PDMS layer, due to the PDMS acting as heat sink. The maximum amplitude of displacement is tied to the stiffness of the bilayer, being inversely correlated to the thickness to the third power. We show that a thin PDMS layer (50 µm) displays almost no hinderance of actuation whereas thicker PDMS layers (130 and 210 µm) show decreased actuation. Additionally, we illustrate that the surface of the splay LCN onto which the PDMS is coated (homeotropic or planar) has a profound effect on the resulting actuation, with coating on the homeotropic surface showing highest actuation potential.

Furthermore, we demonstrate the advantage of combining a PDMS layer with photoresponsive LCN actuators as an approach to incorporate additional triggered responses. Through incorporation of magnetic fillers in the PDMS layer, we demonstrate a bilayer system with untethered photothermal and magnetic response. The bilayer shows increased flexibility in actuation motions, with light triggered bending and magnetic triggered rotational motion. Additionally, bending motion can also be triggered through magnetic stimulus by exposing the bilayer to a strong magnetic field, causing induction heating of the sample due to the magnetic PDMS layer. Through induction heating, the LCN will deform from a bent to a flat state (Figure 2); magnetically triggered bending can be important in applications in which light is not a viable stimulus, such as in enclosed spaces when light penetration is poor. This work provides a design toolbox and a novel approach for future bilayer multi-stimuli responsive actuators which can find applications in a variety of fields including soft robotics and medical applications.

4. Experimental Section

Bilayer Preparation: The liquid crystal polymer network is produced by the photo-copolymerization of two liquid crystalline monomers (Figure S1, Supporting Information), a monoacrylate, M2, (RM 23; 40.5 mol%, Merck) and a diacrylate, M1, (RM 82; 56.5 mol%, Merck), and initiated by a photoinitiator, P.I, (Irgacure 819, 1 mol%, Ciba). Light responsivity was achieved with the addition of a commercially available azo-benzene chromophore with a fast cis-trans isomerization, DR1A, **A1**, (Figure 1A, 2 mol%, Sigma Aldrich). Prior to polymerization, the monomers were dissolved in dichloromethane (DCM) to obtain a homogeneous mixture, the solvent was subsequently evaporated. Polymerization was carried out in a custom-made glass cell prepared by gluing together two glass slides, with 20 µm diameter glass bead spacers incorporated into the glue to achieve controlled cell thickness. Prior to cell fabrication, the individual glass slides were coated with polyimide alignment layers; for a splay alignment one slide employed planar and the other homeotropic alignment layers, Optimer AL 1051 (JSR Micro) and 5661 polyimide (Sunever), respectively. The cells were filled at 95 °C, at which the LC mixture is isotropic, with the LC mixture through capillary action. The filled cell was then cooled to 80 °C, at which temperature the LC mixture is nematic. Photopolymerization of the reactive mesogens was done at this temperature with an Exfo Omnicure S2000 lamp; subsequent thermal treatment at 120 °C for 10 min released thermal stresses arising from polymer shrinkage during polymerization. After polymerization, the cell was opened, and the films peeled from the glass with razor blades and cut into long strips, in which the alignment direction of the planar side is parallel to the long side of the film.

The magnetically functionalized PDMS composite was obtained through manual mixing of a two-component PDMS polymer (Dow Corning) with carbonyl iron powder (Sigma Aldrich) in a 1:1 weight ratio. After degassing the mixture, PDMS composite/LCN bilayers were fabricated by blade coating (thicknesses of 50, 130 and 210 µm) or spin coating at 300 s rpm for 30 s (thickness 35 µm) the uncured PDMS composite onto the photopolymerized LCN film; curing of the PDMS was performed at 80 °C for 1 h. The PDMS was coated on the homeotropic surface of the splay aligned LC film and for the coating process, the LCN was stuck onto a glass substrate as to provide a flat surface for the coating.

Actuation Analysis of the Bilayer Actuators: High speed thermal analysis was performed using a Gobi camera from Xenics. The set-up (Figure S5, Supporting Information) included a blue light of 455 nm (Thorlabs M455L3-C2) with collimation adapter to actuate the samples. Every sample was placed at 9 cm distance from the collimator adapter. A red light-emitting diode (LED) of 617 nm (Thorlabs LED4D100) at a constant low intensity was used to illuminate the sample in the dark for optimal contrast: this wavelength is outside of the absorption spectrum of the LC films. An LED driver (Thorlabs DC4104) allowed for alteration of the light energy output. The recording was processed by a Raspberry Pi model 3B equipped with a Raspberry Pi camera module V2.1 extended with a Fujinon HF25SA-1 camera lens for manually adjustable focus. All samples were placed in such a way that both lights irradiated the sample from the same side (planar surface). A glass box is placed over the sample to prevent airflow influences. A black velvet cloth was placed behind the sample to enhance the contrast.

Incident Energy Calculation: Integrating sphere measurements determined the total amount of energy provided by the LED light beam to a LC film 5.3 mm wide. However, the LC film differed in shape when different incident energies were applied. To compare the absolute response for the equilibrium position at each intensity, a correction was applied for the actual area of the illuminated surface. There were corrections performed (Figure S7, Supporting Information) for either surface loss due to the sample being in a curled position, surface loss due to the sample being out of the beam or beam loss due to the sample being in the beam. These features were all determined by analysis of the images.

Induction Heating Experiment: The induction heating experiment was conducted using a high frequency generator (Sinus 51, 5 kW, 1 MHz), equipped with a 3-turn pancake coil with a radius of 30 mm. The coil and specimen were separated by Teflon foil and the coupling distance was fixed at 1 mm. The strength of the magnetic field applied was of 800 Oe. Sample temperature was monitored with an infrared camera.

Supporting Information

Supporting Information is available from the Wiley Online Library or from the author.

Acknowledgements

The research was made possible by a grant of Technology Foundation STW and the Impuls 2 program of the TU/e. The manuscript was written through contributions of all authors. All authors have given approval to the final version of the manuscript.

Conflict of Interest

The authors declare no conflict of interest.

Keywords

actuators, magnetic response, photoresponse, stimuli-responsive materials

Received: November 20, 2018
Revised: January 8, 2019
Published online:

[1] M. A. C. Stuart, W. T. S. Huck, J. Genzer, M. Müller, C. Ober, M. Stamm, G. B. Sukhorukov, I. Szleifer, V. V. Tsukruk, M. Urban, F. Winnik, S. Zauscher, I. Luzinov, S. Minko, *Nat. Mater.* **2010**, *9*, 101.
[2] S. Nocentini, C. Parmeggiani, D. Martella, D. S. Wiersma, *Adv. Opt. Mater.* **2018**, *6*, 1800207.
[3] H. K. Bisoyi, A. M. Urbas, Q. Li, *Adv. Opt. Mater.* **2018**, *6*, 1800458.
[4] F. D. Jochum, P. Theato, *Chem. Soc. Rev.* **2013**, *42*, 7468.
[5] Y. Liu, B. Shaw, M. D. Dickey, J. Genzer, *Sci. Adv.* **2017**, *3*, e1602417.
[6] G. Kocak, C. Tuncer, V. Bütün, *Polym. Chem.* **2017**, *8*, 144.
[7] J. Thévenot, H. Oliveira, O. Sandre, S. Lecommandoux, *Chem. Soc. Rev.* **2013**, *42*, 7099.
[8] L. Hines, K. Petersen, G. Z. Lum, M. Sitti, *Adv. Mater.* **2017**, *29*, 1603483.
[9] S. I. Rich, R. J. Wood, C. Majidi, *Nat. Electron.* **2018**, *1*, 102.
[10] H. Zeng, P. Wasylczyk, D. S. Wiersma, A. Priimagi, *Adv. Mater.* **2018**, *30*, 1703554.
[11] H. Li, G. Go, S. Y. Ko, J. O. Park, S. Park, *Smart Mater. Struct.* **2016**, *25*, 027001.
[12] A. S. Hoffman, *Adv. Drug Delivery Rev.* **2013**, *65*, 10.
[13] M. Moirangthem, A. P. H. J. Schenning, in *Liquid Crystal Sensors* (Eds: A. P. H. J. Schenning, D. J. Broer, G. P. Crawford), CRC Press, Boca Raton, FL **2018**, pp. 83–102.
[14] J. Hu, H. Meng, G. Li, S. I. Ibekwe, *Smart Mater. Struct.* **2012**, *21*, 053001.
[15] G. V. Stoychev, L. Ionov, *ACS Appl. Mater. Interfaces* **2016**, *8*, 24281.
[16] Q. Li, *Intelligent Stimuli-Responsive Materials: From Well-Defined Nanostructures*, Wiley, Hoboken, NJ, USA **2013**.
[17] M. Wang, B. P. Lin, H. Yang, *Nat. Commun.* **2016**, *7*, 13981.
[18] T. J. White, D. J. Broer, *Nat. Mater.* **2015**, *14*, 1087.
[19] D. Corbett, M. Warner, *Liq. Cryst.* **2009**, *36*, 1263.
[20] K. D. Harris, R. Cuypers, P. Scheibe, C. L. van Oosten, C. W. M. Bastiaansen, J. Lub, D. J. Broer, *J. Mater. Chem.* **2005**, *15*, 5043.
[21] H. Zeng, O. M. Wani, P. Wasylczyk, A. Priimagi, *Macromol. Rapid Commun.* **2018**, *39*, 1700224.
[22] A. H. Gelebart, G. Vantomme, E. W. Meijer, D. J. Broer, *Adv. Mater.* **2017**, *29*, 1606712.
[23] T. J. White, N. V. Tabiryan, S. V. Serak, U. A. Hrozhyk, V. P. Tondiglia, H. Koerner, R. A. Vaia, T. J. Bunning, *Soft Matter* **2008**, *4*, 1796.
[24] G. N. Mol, K. D. Harris, C. W. M. Bastiaansen, D. J. Broer, *Adv. Funct. Mater.* **2005**, *15*, 1155.
[25] H. Shahsavan, S. M. Salili, A. Jákli, B. Zhao, *Adv. Mater.* **2017**, *29*, 1604021.
[26] L. T. De Haan, V. Gimenez-Pinto, A. Konya, T. S. Nguyen, J. M. N. Verjans, C. Sánchez-Somolinos, J. V. Selinger, R. L. B. Selinger, D. J. Broer, A. P. H. J. Schenning, *Adv. Funct. Mater.* **2014**, *24*, 1251.
[27] K. D. Harris, C. W. M. Bastiaansen, D. J. Broer, *J. Microelectromech. Syst.* **2007**, *16*, 480.
[28] L. T. De Haan, J. M. N. Verjans, D. J. Broer, C. W. M. Bastiaansen, A. P. H. J. Schenning, *J. Am. Chem. Soc.* **2014**, *136*, 10585.
[29] M. Winkler, A. Kaiser, S. Krause, H. Finkelmann, A. M. Schmidt, *Macromol. Symp.* **2010**, *291–292*, 186.
[30] S. Herrera-Posada, C. Mora-Navarro, P. Ortiz-Bermudez, M. Torres-Lugo, K. M. McElhinny, P. G. Evans, B. O. Calcagno, A. Acevedo, *Mater. Sci. Eng. C* **2016**, *65*, 369.
[31] Y. Zhan, J. Zhao, W. Liu, B. Yang, J. Wei, Y. Yu, *ACS Appl. Mater. Interfaces* **2015**, *7*, 25522.
[32] F. Cheng, R. Yin, Y. Zhang, C.-C. Yen, Y. Yu, *Soft Matter* **2010**, *6*, 3447.
[33] M. Yamada, M. Kondo, J. I. Mamiya, Y. Yu, M. Kinoshita, C. J. Barrett, T. Ikeda, *Angew. Chem., Int. Ed.* **2008**, *47*, 4986.
[34] M. Dai, O. T. Picot, J. M. N. Verjans, L. T. De Haan, A. P. H. J. Schenning, T. Peijs, C. W. M. Bastiaansen, *ACS Appl. Mater. Interfaces* **2013**, *5*, 4945.
[35] R. C. P. Verpaalen, M. G. Debije, C. W. M. Bastiaansen, H. Halilović, T. A. P. Engels, A. P. H. J. Schenning, *J. Mater. Chem. A* **2018**, *6*, 17724.
[36] A. Agrawal, T. Yun, S. L. Pesek, W. G. Chapman, R. Verduzco, *Soft Matter* **2014**, *10*, 1411.
[37] B. Y. S. Timoshenko, *J. Opt. Soc. Am.* **1925**, *11*, 233.
[38] M. Pilz da Cunha, Y. Foelen, R. J. H. van Raak, J. N. Murphy, A. P. Tom, M. G. Debije, A. P. H. J. Schenning, *Adv. Opt. Mater.* **2019**, *7*, 1801643.
[39] C. L. Van Oosten, K. D. Harris, C. W. M. Bastiaansen, D. J. Broer, *Eur. Phys. J. E* **2007**, *23*, 329.
[40] K. M. Lee, H. Koerner, R. A. Vaia, T. J. Bunning, T. J. White, *Macromolecules* **2010**, *43*, 8185.